Catalysis Communications 147 (2020) 106150

Contents lists available at ScienceDirect

Catalysis Communications

journal homepage: www.elsevier.com/locate/catcom

Short communication

Copper supported Mg—Al hydrotalcite derived oxide catalyst for enol carbamates synthesis via C—H bond activation of formamides

Rakhi Vishwakarma[a], Chandrakanth Gadipelly[a,c], Akhil Nakhate[a,b], Gunjan Deshmukh[a], Lakshmi Kantam Mannepalli[a,*]

[a] Department of Chemical Engineering, Institute of Chemical Technology, Nathalal Parekh Marg, Matunga, Mumbai 400019, India
[b] Department of Chemistry, Bajaj College of Science, Wardha 442001, India
[c] The Wolfson Faculty of Chemical Engineering, Technion-Israel Institute of Technology, Haifa 3200003, Israel

ARTICLE INFO

Keywords:
Copper supported catalyst
Heterogeneous catalyst
Carbamate
Oxidative coupling
C—H bond activation

ABSTRACT

A series of different copper supported Mg—Al—HT derived oxide catalysts have been synthesized by co-precipitation method followed by wet impregnation and calcination. The prepared catalysts were used for enol carbamate synthesis via C—H bond activation of dimethylformamide with ethyl acetoacetate. 15% Cu/Mg—Al—HT derived oxide was the best catalyst with 89% conversion towards ethyl acetoacetate at 100 °C using TBHP as an oxidizing agent. The fresh and spent catalysts have been characterized by XRD, SEM, physisorption, FTIR, TPR-TPD, and XPS. Cu/Mg—Al—HT derived oxide catalyst showed reusability without loss in catalytic activity for three cycles.

1. Introduction

Carbamates are of remarkable interest due to their wide application in various industries, for example in agrochemicals where they are utilized as herbicides, fungicides and pesticides, as drug intermediates in the pharmaceutical industry, for the production of polyurethanes in the polymer industries and in peptide synthesis [1]. Carbamates are used due to their chemical stability towards acids, bases, and hydrogenation. They contain excellent pharmaceutical properties such as antibacterial, neuroprotective, antineoplastic, and anti-filarial agents. There are various green alternative routes for carbamate synthesis like transesterification of substituted urea [2], oxidative carbonylation of amines [3], reductive carbonylation of nitro compounds [4], and methoxy carbonylation of amines [5,6]. A practical method is described for the synthesis of polyurea derivatives from CO_2 and diamines in the absence of the catalysts, and the resulted urea derivatives further reacted with dialkyl carbonates to afford N-substituted dicarbamates using MgO—ZnO catalyst [7]. Formamides are known to react differently under different reaction conditions, as summarized by Muzart in his review, that dimethylformamide is the most widely used derivative which can be a source of oxygen, CO, Me_2NCO, Me_2N and is vital in organometallic chemistry, catalysis and organic synthesis [8]. Not only it is an effective polar solvent, but due to its structure, it is also used as a multipurpose reagent in many reactions. Direct C—H bond activation of formamides has been studied by aminocarbonylation of aryl halides using transition metal catalysts with DMF [9]. Metal-free C—H bond activation has been achieved by direct amidation of azoles with formamides using tertbutyl perbenzoate. Wang and coworkers achieved a possible synthesis of a free radical of dimethylformamide under peroxide conditions. [10] Direct coupling of β-dicarbonyl- or 2-carbonyl-substituted phenols with N, N′-disubstituted formamides under oxidative conditions is also used for carbamate synthesis [11]. Aromatic amides are produced by the coupling of formamides with aryl halides using palladium catalysts in the presence of phosphoryl chloride as an additive. [12] Earlier, we synthesized a series of HT-derived oxide catalysts (Cu—Al, Cu—Fe, Mg—Al, Mg—Fe, Ni—Fe and Ni—Al) from the parent HT–like material followed by calcination and studied their activity for the model reaction of the amidation of carboxylic acids with DMF using TBHP as an oxidant and also the amidation of substituted benzaldehydes [13].

Transition-metal-catalyzed cross-coupling reactions are considered as potent methods for carbon-heteroatom bond formation. Palladium complexes are recognized to be the efficient catalysts for this reaction. Therefore, taking this study forward, we evaluated other transition - metal catalysts, copper-based coupling reactions [14]. There are reports on the formation of aryl carbamates by the reaction of aryl boronic acids with potassium cyanate in the presence of alcohol using a copper catalyst.

* Corresponding author.
E-mail address: lk.mannepalli@ictmumbai.edu.in (L.K. Mannepalli).

https://doi.org/10.1016/j.catcom.2020.106150
Received 27 March 2020; Received in revised form 20 August 2020; Accepted 23 August 2020
Available online 26 August 2020

The cost of homogeneous transition metal-catalyzed cross-coupling reactions and its single-use often restricts its usage. Therefore, heterogeneous catalytic systems have been gained importance for the synthesis of enol carbamates and amides [15,16]. Investigation of copper nanoparticles on charcoal for the synthesis of enol carbamates and amides by the oxidative coupling of N, N-dialkylformamides with 1,3-dicarbonyl compounds and amine hydrochloride salts with aromatic aldehydes, respectively was carried out [17].

Hydrotalcites (Mg_6Al_2 (OH) $_{16}$ CO_3.$4H_2O$) are a class of solid bases which have been used widely for many organic reactions [18–21]. Mixed magnesium-aluminum oxides are formed with a large surface area consisting of acidic and basic sites when hydrotalcites are calcined at 500 °C. Acidic and basic properties can be adjusted by varying metal and metal composition [22].

We began this work with the synthesis of magnesium aluminum hydrotalcite (Mg−Al−HT) derived oxide as reported by Kantam et al. [23], which was further loaded with copper with varying amounts as per the procedure reported by Benito et al. [24] Then, we moved towards the anticipation of DMF activation under oxidative conditions to synthesize the coupled product with carbon nucleophiles using different copper loaded Mg−Al−HT derived oxides to determine the best catalyst for the reaction. For our preliminary experiments, ethyl acetoacetate was chosen as carbon nucleophile and treated with an excess of DMF and, in the presence of 15% Cu on Mg−Al−HT derived oxide catalyst and TBHP (70% in water) as an external oxidant (Scheme 1).

2. Experimental

Please See Supplementary Information.

3. Catalyst characterization

3.1. XRD analysis

The XRD of calcined Mg−Al−HT and copper supported Mg−Al−HT derived oxide catalysts (5% Cu/Mg−Al−HT, 10% Cu/Mg−Al−HT, 15% Cu/Mg−Al−HT, and 20% Cu/Mg−Al−HT) gives a crystalline structure as shown in Fig. SI-1 (Supplementary Information, Fig. 1). Calcined Mg−Al−HT shows reflections at 11°, 23°, 34°, 38°, 43°, and 62° and planes corresponding are (003), (006), (012), (015), (200) and (220), respectively Fig. SI-1a. Mixed oxides are formed from layered double hydroxides by the new broad deflections present at 43° and 62°, which correspond to (200) and (220) planes, respectively [25]. The lattice of MgO and Al_2O_3 were found to be as face-centered cubic and rhombohedral. Calcined Mg−Al−HT is compared with the supported copper Mg−Al−HT derived oxide catalysts made with the increasing concentration of copper in the range of 5, 10, 15, and 20% wt. loading respectively. The presence of copper oxide was in the form of base-centered monoclinic and was seen to increase in the XRD pattern by a sharp peak which goes descending with the increase in the concentration of copper as shown in the figure. Mg−Al−HT derived oxide showed newer peaks having 2θ values of 35°, 39°, 49°, 54°, 58°, 62°, 66°, 68°, 75° which correspond to the CuO phase in the material [26].)

3.2. FTIR studies

The FTIR of calcined Mg−Al−HT and copper supported Mg−Al−HT derived oxide catalysts (5% Cu/Mg−Al−HT, 10% Cu/Mg−Al−HT, 15% Cu/Mg−Al−HT, and 20% Cu/Mg−Al−HT) are shown in Fig. SI-2 (Supplementary Information, Fig. 2). Hydrotalcite formation was confirmed by stretching of hydrogen bonding between the brucite layers with an absorption band at 3425 cm^{-1} as shown in Fig. SI-2a. The peak at 1367 cm^{-1} determines interlayer carbonates. The low-frequency band at 756 cm^{-1} and 623 cm^{-1} corresponds to Al−O and Mg−O. The double absorption band at 1049–997 cm^{-1} for samples (c), (d) and (e) was caused by the significant symmetry of CO_3^{2-}. This dual-band was less in the sample (c) than (d) and (e) [27].

3.3. Nitrogen adsorption-desorption isotherm

The Brunauer-Emmett-Teller (BET) surface area of calcined Mg−Al−HT derived oxide was measured to be 189.2 m^2/g, and the pore volume and pore size was 0.748 cc/g and 18.6 nm, respectively. Surface area analysis data for 5%, 10%, 15%, and 20% of Cu on Mg−Al−HT derived oxides are compared and illustrated in Fig. SI-3 (Supplementary Information, Fig. 3) below. The nitrogen adsorption-desorption isotherm for Mg−Al−HT derived oxide, and supported Cu/Mg−Al−HT found to be type IV with the characteristic of mesoporous material having a small plateau at high relative pressure. The BET surface area (SBET) along with the pore size and pore volume of Mg−Al−HT derived oxide, and the other Cu supported catalysts have been represented in Table SI-1 (Supplementary Information, Table SI-1). It is evident from the data that with an incremental copper loading there is decrease in the pore volume and surface area because of the regional pore-blocking due to the sintering/aggregation of copper species and/or collapse of the lamella due to the calcination temperature. [28,29] The most efficient catalyst 15% Cu supported Mg−Al−HT derived oxide showed a larger surface area compared to lower Cu supported catalyst which might be due to the formation of new surface adsorption sites facilitated from the high dispersion of Cu on the hydrotalcite surface. The decrease in surface area for catalyst with 20% copper loading may be due to aggregation of the copper species and is evident from the decrease in the pore size and pore volume. The copper is very well dispersed in the hydrotalcite materials is also observed in the elemental mapping and similar observation has been reported earlier. [13]

3.4. Microscopic analysis (SEM, EDS and HRTEM)

The surface morphology and elemental analysis of calcined Mg−Al−HT and copper supported Mg−Al−HT derived oxide catalysts was done by SEM and EDS, respectively. Fig. SI-4 (Supplementary Information, Fig. SI-4) shows the apparent difference in the morphology of Mg−Al−HT and copper supported Mg−Al−HT derived oxide analyzed by SEM. The calcined Mg−Al−HT shows an aggregate of a small particle with a smooth surface and in copper supported Mg−Al−HT derived oxide showed the rough surface with the agglomeration of copper nanoparticles. EDS was done for confirmation of aluminum, copper, and magnesium which remain constant in the synthesized catalyst. Furthermore the TEM analysis of calcined Mg−Al−HT and copper supported materials supports the observation of pore blockages due to deposition of copper into the Mg−Al−HT pores and surface Fig. SI-5a & 5b (Supplementary Information, Fig. SI-5) Also, the SAED pattern, (Fig. SI-5c & 5d) shows a perfect crystalline phase of the supported catalyst with array of the Mg−Al−HT catalyst having copper. Fig. SI-6 (Supplementary Information, Fig. SI-6) shows the elemental

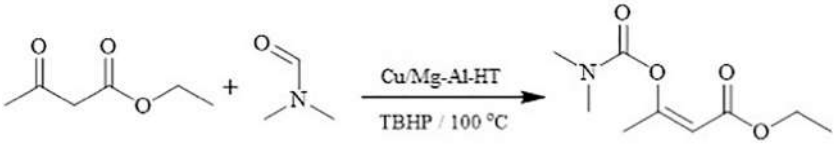

Scheme 1. Enol carbamate synthesis of ethylacetoacetate with formamide using Cu supported Mg−Al−HT derived oxide catalyst using TBHP as an oxidant at 100 °C

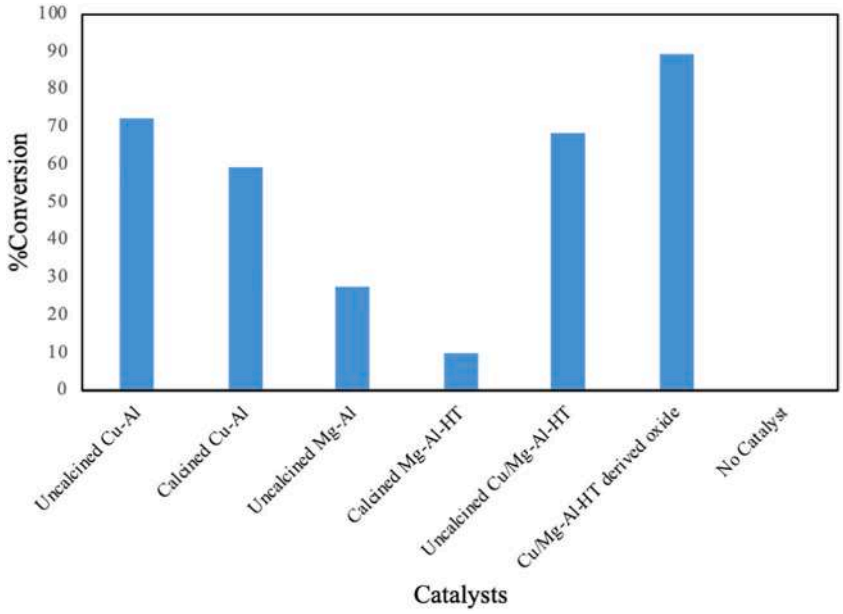

Fig. 1. Screening of various catalysts prepared for enol carbamate synthesis.

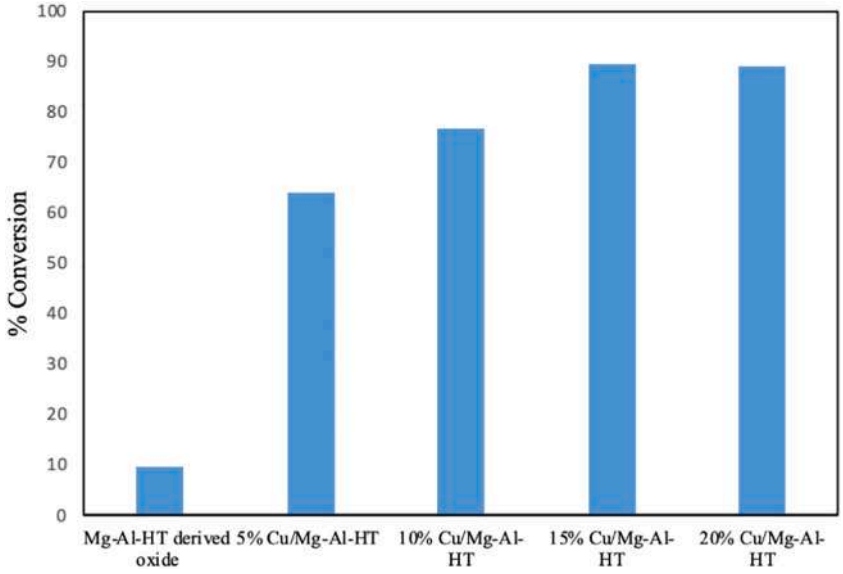

Fig. 2. Effect of copper loading on Cu supported Mg-Al-HT derived oxides [Reaction conditions: EAA (1 mmol.), Catalyst (10 wt% w.r.t. to EAA), DMF (2 mL), TBHP (1.5 equiv.), 100 °C, 12 h].

mapping image of the catalyst which shows an even distribution of copper species (white dots) over the Mg—Al—HT derived oxide. It can be concluded from the figure that the copper has evenly dispersed on the surface of hydrotalcite derived oxide.

3.5. XPS analysis

X-ray photoelectron spectroscopy (XPS) analysis was done to obtain the chemical state of the active metal copper present in the Cu/Mg—Al—HT derived oxide. The survey spectrum Fig. SI-7a (Supplementary Information, Fig. SI-7) clearly indicates the presence of Cu, Mg, and Al in the mixed metal oxide phase. The high-resolution scan of a fresh sample of the catalyst which indicates Cu 2p shown in Fig. SI-7b (Supplementary Information, Fig. SI-7) contains peak at binding energies of 934 eV (Cu $2p_{3/2}$) and 954 eV (Cu $2p_{1/2}$) which concludes the presence of copper in +2 oxidation state. Al 2p core level spectra exhibit a single component and the Al 2p binding energy was observed at 74.48 eV, which is the characteristic photoemission peak of alumina phase Presence of shake up satellite peaks of the Cu 2p core level at 942.5 and 962.6 eV, respectively confirmed the formation of Cu^{2+} on the surface The XPS data of the catalyst after the reaction was also studied to understand the stability of the catalyst. There is no significant change observed seen in the high-resolution scan of used catalyst as shown in Fig. SI-7c & d (Supplementary Information, Fig. SI-7). [27]

3.6. TPR and TPD studies

Temperature programmed reduction studies with H_2 were performed for Mg—Al—HT derived oxides and their subsequent Cu supported Mg—Al—HT derived oxides showed reduction of copper moiety in the temperature range from 200 °C to 340 °C with two sharp peaks at 210 °C and 315 °C showing maximum consumption of hydrogen [30], which signifies the reduction of Cu^{2+} to Cu^0 in two stages. The first

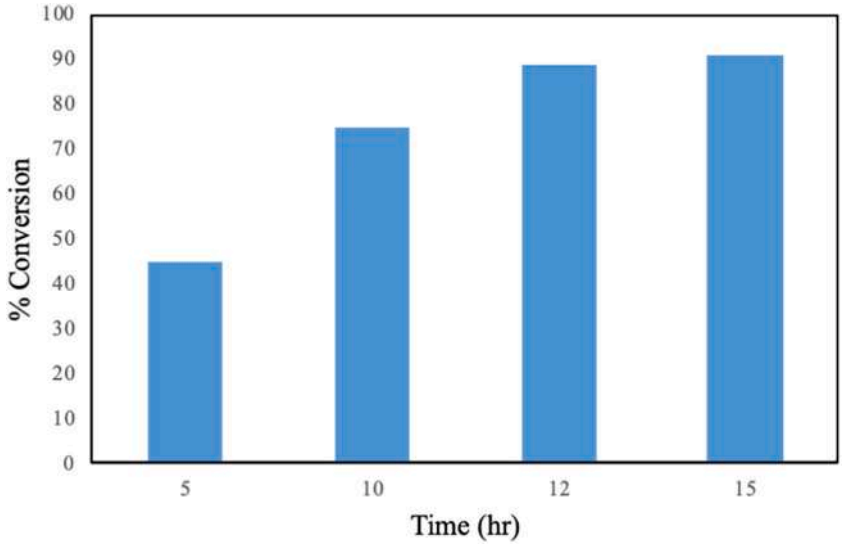

Fig. 3. Effect of reaction time [Reaction conditions: EAA (1 mmol.), Catalyst (10 wt% w.r.t. to EAA), DMF (2 mL), TBHP (1.5 equiv.), 100 °C].

Table 1
Screening of various as-synthesized catalyst for enol carbamate reaction[a].

Sr. No	Catalyst	% Yield
1	Uncalcined Cu–Al	72
2	Calcined Cu–Al	59
3	Uncalcined Mg–Al	28
4	Calcined Mg–Al–HT	10
5	Uncalcined Cu/Mg–Al–HT	68
6	Cu/Mg–Al–HT derived oxide	89

[a] Reaction condition: EAA (1 mmol.), Catalyst (15%), DMF 2 mL, TBHP (1.5 equiv.) 100 °C 12 h.

peak at 210 °C is attributed to the reduction of the highly dispersed Cu phase from Cu^{2+} to Cu^{+} phase and the second sharp peak if the final reduction of Cu^{+} to Cu^{0} phase. The amount of hydrogen consumed per gram and per meter square is presented in Table SI-2 (Supplementary Information, Table SI-2). As the copper concentration increased, there was an increase in hydrogen consumption. This also points to the strong interaction of the copper species to the hydrotalcite support. [26,31]

CO_2 temperature-programmed desorption studies of the catalysts were carried to understand the strength and concentration of basic sites present on the surface. In all the catalysts analyzed, three types of desorption bands were observed, which attributed to the weak, medium, and strong basic strength during desorption in the temperature range from 100 to 600 °C. In all cases, a broad desorption band is observed between 100 °C and 460 °C, which can be deconvoluted into three contributions at about 165 °C (weak basic strength), 200 °C (medium basic strength) and 255 °C (high basic strength). The low-temperature desorption peak corresponds to basic surface OH^{-} groups. The medium temperature peak can be ascribed to $Mg^{2+}–O^{2-}$, $Al^{3+}–O^{2-}$ and $Cu^{2+}–O^{2-}$ acid-base pairs. The high-temperature peak is usually attributed to the strong basic sites associated with low coordinated O^{2-} anions. The amount of CO_2 desorbed represented by these features allows estimating the number of basic sites of the samples. In calcined Mg–Al–HT derived oxide, the basicity was observed to be significantly higher (total basic site density: 5.21 mmol CO_2/g) as compared to copper loaded Mg–Al–HT derived oxides. It is reported that calcination of as-synthesized hydrotalcite gives a well-dispersed mixture of Mg and Al mixed oxides having strong Lewis (isolated O^{2-} anions) and weaker Brønsted (OH^{-} groups) basic sites [31]. The basicity of the catalytic material decreased on copper loading to the Mg–Al–HT derived oxide, and there was no substantial change in the basicity observed with an increase in the copper concentration.

4. Catalytic activity

Initially, screening of different calcined and uncalcined hydrotalcite was carried out under the same reaction conditions, Ethyl acetoacetate [EAA] (1 mmol, limiting reagent), catalyst (15% w.r.t. limiting reagent), dimethyl formamide [DMF] (2 mL), tert-Butyl hydrogen peroxide [TBHP] (1.5 equiv.) at 100 °C 12 h. The influence of different hydrotalcite on the yield of enol carbamate was comparatively analyzed.

The reaction was carried out with calcined and uncalcined Mg–Al–HT with and without copper support, along with other copper-aluminum catalysts prepared by co-precipitation techniques for comparison and understanding the role of copper. As mentioned in Table 1 and Fig. 1, Cu/Mg–Al–HT derived oxide was found to be the best for enol carbamate synthesis, whereas no product formation was seen without the catalyst. Cu–Al catalyst (calcined or uncalcined) also showed lower conversions in comparison to the HT based catalyst as in the former Cu species are in bulk form whereas in later the copper species are very well dispersed into the hydrotalcite structure making the Cu ions more accessible. Also, in the catalyst preparation method, catalyst synthesized by wet-impregnation of copper species in alcoholic medium was found to be more efficient as compared to impregnation in aqueous medium which gave 79% conversion only. This is due to the excellent dispersion of copper ions in the HT support in alcoholic medium as the metal species diffuse very well as compared to aqueous medium. [32] So, we can conclude that basic supports (hydrotalcite and its derived mixed oxide) are found to be suitable for copper to promote its catalytic activity for C–H bond activation for enol carbamate synthesis.

With Cu supported Mg–Al–HT derived oxide catalyst as the best suited material for enol carbamate synthesis, further screening was studied to understand the effect of copper loading on the catalytic activity. No conversion was seen when native Mg–Al–HT derived oxide was used, and an increase in conversion was observed with an increase in the percentage of copper concentration on the support as shown in Fig. 2. The catalytic yield for 15 wt% and 20 wt% Cu supported Mg–Al–HT derived oxide showed no significant change with both showing conversions of 89% respectively. Thus, 15 wt% Cu supported Mg–Al–HT derived oxide was considered to be an efficient catalyst and used for further optimizations. In order to study the role of oxidant, we used 1.5 equiv. of TBPB (tert-butyl peroxy benzoate) as an oxidant, 5% conversion was observed. Whereas, we observed no product formation when TBHP in 5.0 M decane was used as an oxidant without catalyst.

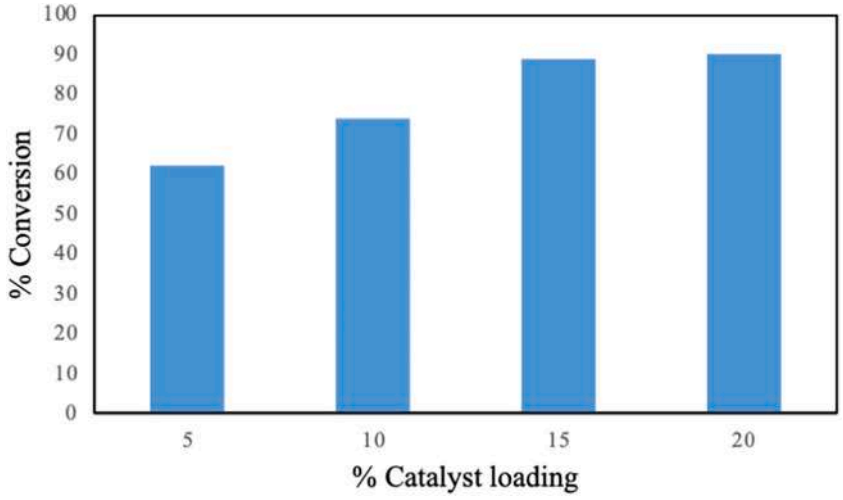

Fig. 4. Effect of catalyst loading. [Reaction conditions: EAA (1 mmol.), DMF (2 mL), TBHP (1.5 equiv.), 100 °C, 12 h].

We determined that TBHP proved to be the best oxidant to synthesize enol carbamates, which is consistent with our previous studies of C—H activation [33].

Further, optimization of the reaction time was monitored from 5 to 15 h. The conversion obtained at different time intervals is shown in Fig. 3. It can be observed that the conversion increases with an increase in reaction time up to 12 h. Further increase in reaction time to 15 h, did not result in any significant increase in conversion, and therefore, 12 h was optimized for further reactions. Different experiments were carried out by varying the reaction temperature from 80 to 100 °C, for studying the temperature effect on oxidative coupling over Cu/Mg—Al—HT derived oxide as shown in Fig. SI-8 (Supplementary Information, Fig. SI-8) Increase in conversion was observed with the increase in temperature and reached a maximum of 89% at 100 °C.

The effect of catalyst loading was studied further and presented in Fig. 4, which shows the varying percent of catalyst used for the reaction from 5 wt% - 20 wt% catalyst with respect to limiting reagent. It was observed that the conversion of limiting reagent increased with increase in catalyst loading. There was no significant conversion observed beyond 15% catalyst loading. The results show that the highest conversion 89% was obtained at 15 wt% of catalyst loading, and the lowest 62% at 5 wt% of 15% Cu/Mg—Al—HT derived oxide catalyst.

4.1. Substrate scope of enol-carbamate

With the reaction conditions optimized, substrate with structural diversity were studied using 15% Cu/Mg—Al—HT derived oxide catalyst at 100 °C with 2 mL of dimethylformamide and diethylformamide as a solvent and TBHP as the external oxidant. Various β-ketoesters were used as substrates under standard reaction conditions for the formation of enol carbamate, as shown in Table SI-3 (Supplementary Information, Table SI-3) We observed that all β-ketoesters were transformed into their corresponding enol carbamates. Excellent conversions were found by using dimethylformamide with various substituted β-ketoesters. However, the active methylene group did not participate in the reaction in the case of 1, 3-cyclohexanedione, which showed lower conversions in comparison to other substrates. Cyclic and bulky formamides provided slightly lower yields, suggesting the negative effect of steric hindrance on the reaction.

Mechanistically, the dicarbonyl functionalities in the β-ketoesters possess the tendency of forming coordination complexes with transition metals as shown in the mechanism, Fig. SI-9 (Supplementary Information, Fig. SI-9). The copper complex then decomposes TBHP to form respective radicals which can further abstract hydrogen from the formamide, generating the corresponding radical. This radical then further reacts with the copper complex to give the desired carbamate [34]. The similar reaction pathway has also been reported by Barve et al. [35]

4.2. Recyclability of the catalyst

After the reaction, the catalyst was filtered and refluxed with 10 mL of methanol and washed with 15 mL methanol to remove any adsorbed material from catalytic surface and pores and then dried at 120 °C. It was also calcined at 450 °C for 8 h and then cooled to room temperature and weighed. Overall there was no loss of catalyst during centrifugation and separation. The same procedure was followed in subsequent experiments. The catalyst was reused for three times without loss in activity, and results are shown in Table SI-4 (Supplementary Information, Table SI-4). Thus, the stability of the synthesized material was confirmed w.r.t. activity. The XRD of the recycled catalyst was compared with the fresh catalyst, and there was no significant change in the catalyst which confirmed the stability of the catalyst. (Supplementary Information, Fig. SI-10).

Also, the catalyst was subjected to hot-filtration method to check for the leaching of the active metals from the catalyst. After the reaction, the reaction vial was opened in the hot condition and filtered quickly using a filter paper. The filtrate collected was diluted with 10 mL of DMF. The prepared sample was given for ICP-OES and copper was not detected in the solution indicating no leaching of copper ions from the catalyst. The yield after removing the catalyst was 89%, which was consistent with the results obtained during the recyclability studies.

5. Conclusion

A simple and efficient procedure was developed for the synthesis of carbamate derivatives over Cu/Mg—Al—HT derived oxide catalysts. Cu/Mg—Al—HT derived oxide catalyst (5%, 10%, 15% and 20% copper loading) is synthesized and characterized by various analytical techniques such as XRD, FTIR, SEM, and N_2 adsorption-desorption. Among all the catalysts, 15% Cu/Mg—Al—HT derived oxide catalyst was found to be active for the synthesis of enol derivatives. Broad substrate study has been done for the synthesis of enol carbamates. The catalyst was recycled up to three cycles and found to be active without any significant loss in activity.

Declaration of Competing Interest

The authors declare that they have no known competing financial interests or personal relationships that could have appeared to

influence the work reported in this paper.

Acknowledgment

MLK gratefully acknowledges support from Godrej Consumer Products Limited (GPCL) for Dr. B. P. Godrej Chair Professor and J.C. Bose National Fellowship (SERB-DST, GoI). Rakhi highly acknowledges the support provided by Science & Engineering Research Board (SERB, GoI). Gunjan, Chandrakanth, and Akhil acknowledge VOL and J.C. Bose Research Grant (SERB-DST, GoI).

Appendix A. Supplementary data

Supplementary data to this article can be found online at https://doi.org/10.1016/j.catcom.2020.106150.

References

[1] A.R. Modarresi-Alam, M. Rostamizahed, P. Najafi, Solvent-free preparation of primary carbamates, Turkish J. Chem. 30 (2006) 269–276.
[2] P. Wang, Y. Fei, Q. Li, Y. Deng, Effective synthesis of dimethylhexane-1,6-dicarbamate from 1,6-hexanediamine and dimethyl carbonate using 3-amino-1,2,4-triazole potassium as a solid base catalyst at ambient temperature, Green Chem. 18 (2016) 6681–6686, https://doi.org/10.1039/c6gc02509a.
[3] B. Chen, S.S.C. Chuang, CuCl2 and PdCl2 catalysts for oxidative carbonylation of aniline with methanol, J. Mol. Catal. A Chem. 195 (2003) 37–45, https://doi.org/10.1016/S1381-1169(02)00550-2.
[4] F. Ragaini, M. Gasperini, S. Cenini, Phosphorus acids as highly efficient promoters for the palladium- phenanthroline catalyzed carbonylation of nitrobenzene to methyl phenylcarbamate, Adv. Synth. Catal. 346 (2004) 63–71, https://doi.org/10.1002/adsc.200303143.
[5] Y. Ono, Catalysis in the production and reactions of dimethyl carbonate, an environmentally benign building block, Appl. Catal. A. Gen. 155 (1997) 133–166, https://doi.org/10.1016/S0926-860X(96)00402-4.
[6] N. Lucas, A.P. Amrute, K. Palraj, G.V. Shanbhag, A. Vinu, S.B. Halligudi, Non-phosgene route for the synthesis of methyl phenyl carbamate using ordered AlSBA-15 catalyst, J. Mol. Catal. A Chem. 295 (2008) 29–33, https://doi.org/10.1016/j.molcata.2008.08.009.
[7] J. Shang, S. Liu, X. Ma, L. Lu, Y. Deng, A new route of CO2 catalytic activation: Syntheses of N-substituted carbamates from dialkyl carbonates and polyureas, Green Chem. 14 (2012) 2899–2906, https://doi.org/10.1039/c2gc36043h.
[8] J. Muzart, N,N-Dimethylformamide: Much more than a solvent, Tetrahedron. 65 (2009) 8313–8323, https://doi.org/10.1016/j.tet.2009.06.091.
[9] J. Ju, M. Jeong, J. Moon, M.J. Hyun, S. Lee, Aminocarbonylation of aryl halides using a nickel phosphite catalytic system, Org. Lett. 9 (2007) 4615–4618, https://doi.org/10.1021/ol702058e.
[10] T. He, H. Li, P. Li, L. Wang, Direct amidation of azoles with formamides via metal-free C-H activation in the presence of tert-butyl perbenzoate, Chem. Commun. 47 (2011) 8946–8948, https://doi.org/10.1039/c1cc13086b.
[11] G.S. Kumar, C.U. Maheswari, R.A. Kumar, M.L. Kantam, K.R. Reddy, Copper-catalyzed oxidative C-O coupling by direct C-H bond activation of formamides: synthesis of enol carbamates and 2-carbonyl-substituted phenol carbamates, Angew. Chem. Int. Ed. 50 (2011) 11748–11751, https://doi.org/10.1002/anie.201105020.
[12] K. Hosoi, K. Nozaki, T. Hiyama, Carbon monoxide free aminocarbonylation of aryl and alkenyl iodides using DMF as an amide source, Org. Lett. 4 (2002) 2849–2851, https://doi.org/10.1021/ol026236k.
[13] P.S. Samudrala, A.V. Nakhate, S.S.R. Gupta, K.B. Rasal, G.P. Deshmukh, C.R. Gadipelly, S. Theegala, D.K. Dumbre, S. Periasamy, V.R.C. Komandur, et al., Oxidative coupling of carboxylic acids or benzaldehydes with DMF using hydrotalicite-derived oxide catalysts, Appl. Catal. Environ. 240 (2019) 348–357.
[14] E. Kianmehr, M.H. Baghersad, Copper-catalyzed coupling of arylboronic acids with potassium cyanate: A new approach to the synthesis of aryl carbamates, Adv. Synth. Catal. 353 (2011) 2599–2603, https://doi.org/10.1002/adsc.201100153.
[15] D. Saberi, A. Heydari, Oxidative amidation of aromatic aldehydes with amine hydrochloride salts catalyzed by silica-coated magnetic carbon nanotubes (MagCNTs@SiO 2)-immobilized imine-Cu(I), Appl. Organomet. Chem. 28 (2014) 101–108, https://doi.org/10.1002/aoc.3087.
[16] S. Ghosh, A. Bhaumik, J. Mondal, A. Mallik, S. Sengupta, C. Mukhopadhyay, Direct amide bond formation from carboxylic acids and amines using activated alumina balls as a new, convenient, clean, reusable and low cost heterogeneous catalyst, Green Chem. 14 (2012) 3220–3229, https://doi.org/10.1039/c2gc35880h.
[17] D. Saberi, S. Mansoori, E. Ghaderi, K. Niknam, Copper nanoparticles on charcoal: An effective nanocatalyst for the synthesis of enol carbamates and amides via an oxidative coupling route, Tetrahedron Lett. 57 (2016) 95–99, https://doi.org/10.1016/j.tetlet.2015.11.072.
[18] G.D. Yadav, G.P. Fernandes, Selective synthesis of natural benzaldehyde by hydrolysis of cinnamaldehyde using novel hydrotalcite catalyst, Catal. Today 207 (2013) 162–169, https://doi.org/10.1016/j.cattod.2012.04.052.
[19] P. Liu, K. You, R. Deng, Z. Chen, J. Jian, F. Zhao, P. Liu, Q. Ai, H. Luo, Hydrotalcite-derived Co-MgAlO mixed metal oxides as efficient and stable catalyst for the solvent-free selective oxidation of cyclohexane with molecular oxygen, Mol. Catal. 466 (2019) 130–137, https://doi.org/10.1016/j.mcat.2019.01.019.
[20] A. López, J.A. Aragón, J.G. Hernández-Cortez, M.L. Mosqueira, R. Martínez-Palou, Study of hydrotalcite-supported transition metals as catalysts for crude glycerol hydrogenolysis, Mol. Catal. 468 (2019) 9–18, https://doi.org/10.1016/j.mcat.2019.02.008.
[21] M.S. Maru, S. Ram, R.S. Shukla, N.H. Khan, Ruthenium-hydrotalcite (Ru-HT) as an effective heterogeneous catalyst for the selective hydrogenation of CO2 to formic acid, Mol. Catal. 446 (2018) 23–30, https://doi.org/10.1016/j.mcat.2017.12.005.
[22] D.P. Debecker, E.M. Gaigneaux, G. Busca, Exploring, tuning, and exploiting the basicity of hydrotalcites for applications in heterogeneous catalysis, Chem. - A Eur. J. 15 (2009) 3920–3935, https://doi.org/10.1002/chem.200900060.
[23] B.M. Choudary, M. Lakshmi Kantam, C. Venkat Reddy, K. Koteswara Rao, et al., Henry reactions catalysed by modified Mg–Al hydrotalcite:. an efficient reusable solid base for selective synthesis of $β$-nitroalkanols, Green Chem. 1 (1999) 187–189.
[24] P. Benito, A. Vaccari, C. Antonetti, D. Licursi, N. Schiarioli, E. Rodriguez-Castellón, A.M. Raspolli Galletti, Tunable copper-hydrotalcite derived mixed oxides for sustainable ethanol condensation to n-butanol in liquid phase, J. Clean. Prod. 209 (2019) 1614–1623, https://doi.org/10.1016/j.jclepro.2018.11.150.
[25] S.L. Bhanawase, G.D. Yadav, Activity and selectivity of different base catalysts in synthesis of guaifenesin from guaiacol and glycidol of biomass origin, Catal. Today 291 (2017) 213–222, https://doi.org/10.1016/j.cattod.2016.12.008.
[26] N. Blanch-Raga, A.E. Palomares, J. Martínez-Triguero, G. Fetter, P. Bosch, Cu mixed oxides based on hydrotalcite-like compounds for the oxidation of trichloroethylene, Ind. Eng. Chem. Res. 52 (2013) 15772–15779, https://doi.org/10.1021/ie4024935.
[27] A.V. Nakhate, G.D. Yadav, Hydrothermal synthesis of CuFe2O4 magnetic nanoparticles as active and robust catalyst for N-arylation of indole and imidazole with aryl halide, ChemistrySelect. 2 (2017) 2395–2405, https://doi.org/10.1002/slct.201601846.
[28] M. Peymani, S.M. Alavi, H. Arandiyan, M. Rezaei, Rational design of high surface area mesoporous Ni/CeO2 for partial oxidation of propane, Catalysts. 8 (2018), https://doi.org/10.3390/catal8090388.
[29] E.M. Fuentes, A. Da Costa Faro, T. De Freitas Silva, J.M. Assaf, M.D.C. Rangel, A comparison between copper and nickel-based catalysts obtained from hydrotalcite-like precursors for WGSR, Catal. Today 171 (2011) 290–296, https://doi.org/10.1016/j.cattod.2011.03.082.
[30] J.S. Valente, J. Hernandez-Cortez, M.S. Cantu, G. Ferrat, E. López-Salinas, Calcined layered double hydroxides Mg-Me-Al (Me: Cu, Fe, Ni, Zn) as bifunctional catalysts, Catal. Today 150 (2010) 340–345, https://doi.org/10.1016/j.cattod.2009.08.020.
[31] M. Dixit, M. Mishra, P.A. Joshi, D.O. Shah, Physico-chemical and catalytic properties of Mg-Al hydrotalcite and Mg-Al mixed oxide supported copper catalysts, J. Ind. Eng. Chem. 19 (2013) 458–468, https://doi.org/10.1016/j.jiec.2012.08.028.
[32] J. De Waele, V.V. Galvita, H. Poelman, C. Detavernier, J.W. Thybaut, PdZn nanoparticle catalyst formation for ethanol dehydrogenation: active metal impregnation vs incorporation, Appl. Catal. A. Gen. 555 (2018) 12–19, https://doi.org/10.1016/j.apcata.2018.02.005.
[33] P.S. Samudrala, A.V. Nakhate, S.S.R. Gupta, K.B. Rasal, G.P. Deshmukh, C.R. Gadipelly, S. Theegala, D.K. Dumbre, S. Periasamy, V.R.C. Komandur, S.K. Bhargava, L.K. Mannepalli, Oxidative coupling of carboxylic acids or benzaldehydes with DMF using hydrotalicite-derived oxide catalysts, Appl. Catal. Environ. 240 (2019) 348–357, https://doi.org/10.1016/j.apcatb.2017.12.058.
[34] D. Saberi, S. Poorsadeghi, Nickel-catalyzed oxidative esterification of formamides with 1,3-dicarbonyl compounds under mild reaction conditions, Appl. Organomet. Chem. 31 (e3855) (2017), https://doi.org/10.1002/aoc.3855.
[35] B.D. Barve, Y. Wu, M. El-Shazly, D. Chuang, Y.-M. Chung, Y.-H. Tsai, S.-F. Wu, M. Korinek, Y.-C. Du, C. Hsieh, J. Wang, F. Chang, Synthesis of carbamates by direct C-H bond activation of Formamides, Eur J. Org. Chem. 2012 (2012) 6760–6766, https://doi.org/10.1002/ejoc.201201160.